KSME

Springer

Journal of Mechanical Science and Technology 36 (12) 2022

Original Article
DOI 10.1007/s12206-022-1109-3

Keywords:
· Agricultural machinery working environment
· Weak characteristic damped oscillation signal
· VR
· VMD
· Grain loss signal

Correspondence to:
Suzhen Wang
sophi99@126.com

Citation:
Wang, S., Lu, B. (2022). Detecting the weak damped oscillation signal in the agricultural machinery working environment by vibrational resonance in the duffing system. Journal of Mechanical Science and Technology 36 (12) (2022) 5925~5937.
http://doi.org/10.1007/s12206-022-1109-3

Received July 14th, 2022
Revised August 7th, 2022
Accepted August 17th, 2022

† Recommended by Editor
No-cheol Park

Detecting the weak damped oscillation signal in the agricultural machinery working environment by vibrational resonance in the duffing system

Suzhen Wang[1,2] and Baochun Lu[1]

[1]Nanjing University of Science & Technology, Nanjing 210094, China, [2]Nanjing Research Institute for Agriculture Mechanization, Ministry of Agriculture and Rural Affairs, Nanjing 210014, China

Abstract The working environment for agricultural machinery is complex and variable. Some weak characteristic damped oscillation signals are extremely difficult to extract and analyze because of their long-term operation in a strong noise environment. The vibration resonance (VR) phenomenon of a second-order Duffing bistable system driven by a weak characteristic damped oscillation signal and a high-frequency harmonic signal was studied. The results indicate that the cooperation between the Duffing damping ratio and attenuation coefficient can induce the VR occurrence of a small-parameter damped oscillation signal. As a result, the energy of the weak characteristic signal becomes stronger, and the VR numerical processing method of the high-frequency weak characteristic damped oscillation signal is provided. On this basis, aiming at the strong noise of agricultural machinery working, taking the weighted kurtosis index as the objective function and supplemented by variational mode decomposition (VMD) technology, a VR-VMD adaptive method based on quantum particle swarm optimization (QPSO) was proposed to extract the weak characteristic damped oscillation signal. Numerical simulation analysis and experiments show that the proposed VR-VMD method is effective in a strong noise environment for agricultural machinery.

1. Introduction

Vibration signals are difficult to detect in long-term agricultural environments. The loss detection signal of the grain combine harvester is a prominent case. Grain combine harvesters are a type of harvesting agricultural machinery that directly obtain grain from the field. They are widely used and can be used to complete the processes of harvesting, threshing, separating stems and rods, and removing impurities. From an economic perspective, grain harvesting losses lead to direct economic losses for farmers. Thus, grain harvesting losses have become one of the main indicators for measuring the operational performance of combine harvesters [1]. When the manipulator is improperly operated or the working parameters of the harvester are inappropriate, a large number of grains do not fall into the cleaning system and enter the vibrating sieve, because the structure and operating parameters of the existing combine harvester are not adaptive. Ultimately, they will be discharged together with the grasses and sundries from the grass outlet and tail of the vibrating sieve, resulting in grain losses.

The loss sensor detects a series of weak damped oscillation signals. The grain loss detection signals are weaker than the vibration noise interference of the harvester and are basically submerged in the background noise and interference (the weak signals are relative to the background noise) owing to the relatively poor grain harvesting environment. Separating the grain cleaning losses from a strong vibration background has always been a difficult problem in harvester research [2]. This has sparked the interest of several researchers. In principle, loss detection requires a sufficiently large signal-to-noise ratio (SNR) at the electrical signal processing input. However, when the SNR at the input of the signal processing system is very unsatis-

factory, corresponding methods must be adopted to separate the signal and noise according to their different characteristics of signal and noise. Ni et al. [3] studied a filter to separate the vibration noise of the machine from the characteristics of grain signals by simulating the strong noise background of the harvester operation indoors. Gao et al. [4] used a Duffing oscillator to extract loss signals under a strong noise background. Mao et al. [5] adopted a symmetrical sensor structure to eliminate the vibration interference in signal loss. The core idea of denoising in these methods is to remove as much background noise from the observed data as possible and leave useful signals. They have been applied in many fields and have shown good results, such as the commonly used analog filters, blind source separation (BSS) [6], wavelet transform [7], empirical modal decomposition (EMD), and Hilbert Huang transform (HHT) [8, 9].

In recent decades, another noise-reduction method has been introduced that is used to enhance the weak signal by reasonably using the background noise or adding an auxiliary high-frequency harmonic signal; it is the so-called noise or high-frequency harmonic utilization mechanism. Among them, stochastic resonance (SR) and vibration resonance (VR) theories are key fields of research. Since Benzi et al. [10] proposed the concept of SR when studying paleoglacial meteorology in 1981, SR has attracted extensive attention in many fields. SR indicates that under the action of a nonlinear system, noise may play a role contrary to people's intuition. That is, a certain amount of noise does not only reduce the output response of the system, but also strengthens the output response of the system to a certain extent. However, under the condition of large noise intensity parameters, such as the working environment of the combine harvester, only an appropriate amount of small noise is required owing to the SR generated by the system. Thus, excessive residual noise can exist only as residual noise and drowns the characteristic signal output of the system. Landa and McClintock [11] proposed the VR theory. When they studied SR, they replaced the noise with a high-frequency harmonic signal and then found another special nonlinear dynamic characteristic, namely VR. The VR system can also obtain a higher SNR than SR [12]. The VR theory has advanced to enhance the energy of the noisy damped oscillation signal and combined with variational modal decomposition (VMD) technology to further improve the SNR of the damped oscillation signal in the agricultural machinery working environment.

The remainder of this paper is arranged as follows: the theoretical and numerical analyses of VR based on second-order Duffing are shown in Sec. 2. See Sec. 3 for VR numerical method of large parameter damped oscillation signal in the project. In Sec. 4, the adaptive extraction method of damped oscillation signal of VR-VMD under noise background is introduced and simulated. In Sec. 5, the VR-VMD method is verified using the noisy weak characteristic loss damped oscillation signal in the agricultural machinery working environment, and the extraction effect is compared with the traditional envelope method; Finally, Sec. 6 draws a conclusion.

2. Models and methods

2.1 VR phenomenon

VR is a resonance phenomenon similar to SR that uses noise to enhance a weak signal. VR enhances weak signal energy by injecting a high-frequency harmonic signal. As the starting point, the VR physical model studied is based on the second-order Duffing oscillator damping model, which is expressed in Eq. (1), as follows:

$$\frac{d^2x}{dt^2}+\gamma\frac{dx}{dt}=-U'(x)+s(t)+H(t) \tag{1}$$

where γ is the damping ratio of the Duffing oscillator, and $s(t)=Ae^{-\lambda(t-nT)}\sin(2\pi f_0 t)$ (nT represents n oscillation periods with T), is the weak damped oscillation signal to be detected. In this section, only the frequency $f_0 << 1$ is considered. where λ is the attenuation coefficient of a weak signal. $H(t)=H\cos(2\pi f_h t)$ is the injected high-frequency cosine excitation periodic signal, where $f_h >> f_0$ and $U(x)=-\frac{1}{2}a_0x^2+\frac{1}{4}b_0x^4$ are the bistable nonlinear potential well functions, and a_0 and b_0 are the two parameters of the system and positive numbers.

According to the method proposed in Refs. [13, 14], the output system $x(t)$ can be decomposed into two motion components: a slow-motion component X and a fast-motion component ψ. Substituting $x=X+\psi$ into Eq. (1) yields

$$\begin{aligned}&\frac{d^2(X+\psi)}{dt^2}+\gamma\frac{d(X+\psi)}{dt}-a_0(X+\psi)\\&+b_0(X+\psi)^3=s(t)+H\cos(2\pi f_h t)\end{aligned} \tag{2}$$

Among them, $\overline{\psi}=<\psi>=\frac{1}{2\pi}\int_0^{2\pi}\psi d\tau=0$. Assuming that the motion speed of ψ is much faster than that of X, Eq. (3) can be obtained as follows:

$$\frac{d^2X}{dt^2}+\gamma\frac{dX}{dt}+C_1X+b_0X^3=s(t) \tag{3}$$

where $C_1=-a_0+\frac{3b_0H^2}{2(2\pi f_h)^4}$.

Eq. (4) is the particle motion Eq. (3) with the effective potential of the system (3).

$$V(X)=\frac{C_1}{2}X^2+\frac{b_0}{4}X^4 \tag{4}$$

The potential of the slow-motion variable X depends on

the parameters of f_h and H of the fast-motion variable ψ. When subjected to nonlinear damping and the driving force $Ae^{-\lambda(t-nT)}\sin(2\pi f_0 t)$, the slow-motion variable X moves near the stable equilibrium points of the driving system (4). Additionally, the equilibrium point of the X variable is the root of this equation, $C_1X^* + b_0X^{*3} = 0$. Among them, $X_1^* = 0$ and $\frac{a_0}{b_0} - \frac{3H^2}{2(2\pi f_h)^4} > 0$, two other stable equilibrium points exist, $X_{2,3}^* = \sqrt{\frac{a_0}{b_0} - \frac{3H^2}{2(2\pi f_h)^4}}$ at that time. According to the H value, the effective potential energy of the slow oscillator changed from double to a single potential well. This bifurcation value $H_c = \sqrt{\frac{2a_0(2\pi f_h)^4}{3b_0}}$ is in the classical vibrational resonance of the Duffing equation [15]. To eliminate the constant component and retain the harmonic term in the response, we substitute $Y = X - X^*$ into Eq. (3) to obtain Eq. (5), as follows:

$$\frac{d^2Y}{dt^2} + \gamma\frac{dY}{dt} + (C_1 + 3b_0X^{*2})Y + 3b_0X^*Y^2 + b_0Y^3 = Ae^{-\lambda(t-nT)}\sin(2\pi f_0 t) \tag{5}$$

$f_0 << 1$; thus, $|Y| << 1$ can be linearized in the neighborhood of the stable equilibrium points to obtain the corresponding linear Eq. (6) as follows:

$$\frac{d^2Y}{dt^2} + \gamma\frac{dY}{dt^2} + \omega_r^2 Y = Ae^{-\lambda(t-nT)}\sin(2\pi f_0 t) \tag{6}$$

where $\omega_r^2 = C_1 + 3b_0X^{*2}$. After a period of motion, the solution $Y = t^k QAe^{-\lambda(t-nT)}\sin(2\pi f_0 t + \Delta_\gamma)$ is obtained, in which k = 0 or 1 is obtained according to $-\lambda + i\omega$ (or $-\lambda - i\omega$) or a single root of the characteristic equation. In addition, the characteristic equation used is $r^2 + \gamma r + \omega_r^2 = 0$. k = 0 because $\lambda\omega \neq 0$. We used the response amplitude index Q to evaluate the effect of VR at low-frequency $\omega = 2\pi f_0$ and derived Eq. (7) as follows:

$$Q = \frac{1}{\sqrt{(\omega_r^2 + \lambda^2 - \omega^2 - \gamma\lambda)^2 + (2\lambda - \gamma)^2\omega^2}} \tag{7}$$

Its value is not only related to the potential well parameters, high-frequency driving excitation signal, and damping ratio but is also affected by the attenuation coefficient of the weak signal.

When λ = 0, classical vibration resonance research [16-19] was completed. Here, we consider only the case of $\lambda > 0$ to study the VR phenomenon. To study the mutual coordination ability of γ and λ, the compound influence factor $d = 2\lambda - \gamma$ was defined, and the response amplitude was redefined as $Q = \frac{1}{\sqrt{(\omega_r^2 + \lambda^2 - \omega^2 - \gamma\lambda)^2 + d^2\omega^2}}$. Fig. 1 shows the

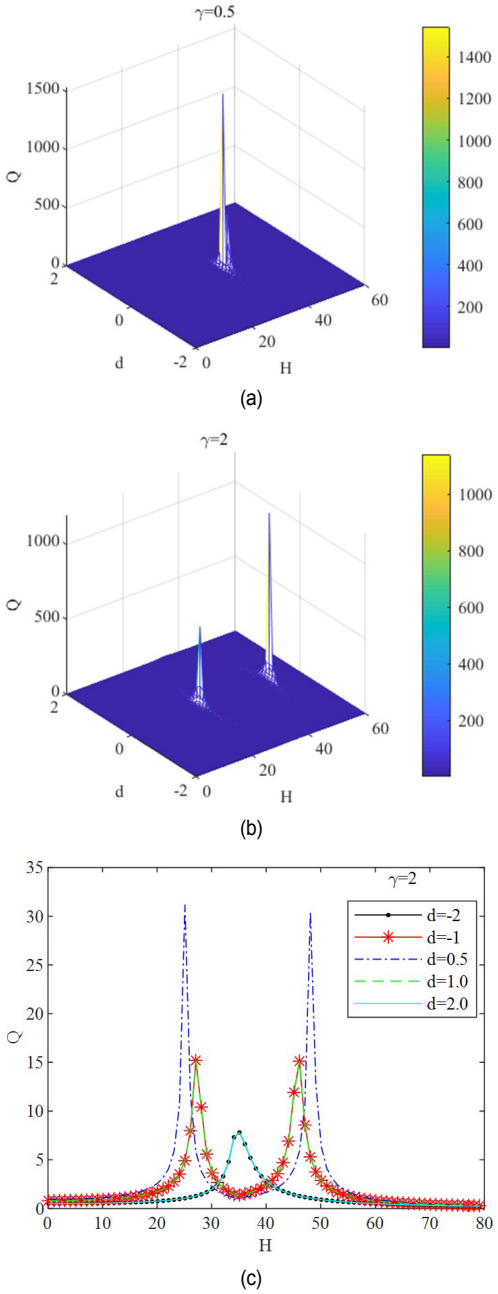

Fig. 1. The VR phenomenon occurs at the frequency $\omega = 2\pi f_0$ for different d values: (a) and (b) 3D curve of the response amplitude Q obtained by the analytical predication; (c) response amplitude versus the signal amplitude H for different d values. Parameters are as follows: $A = 0.1$, $f_0 = 0.01$, $f_h = 1$ and $a_0 = b_0 = 1$.

VR analysis results for different values of d for different damping ratios γ. The other parameter configurations are as follows: A = 0.1, f_0 = 0.01, f_h = 1 and $a_0 = b_0 = 1$. In Fig. 1, the response amplitude Q initially increases with the increase in H and then decreases after reaching the peak. Two resonances are obtained when $\gamma < |d|$ and when d = 0, a symmetrical output effect is formed simultaneously. Figs. 1(a) and (b) show that the distance between the two formants increases

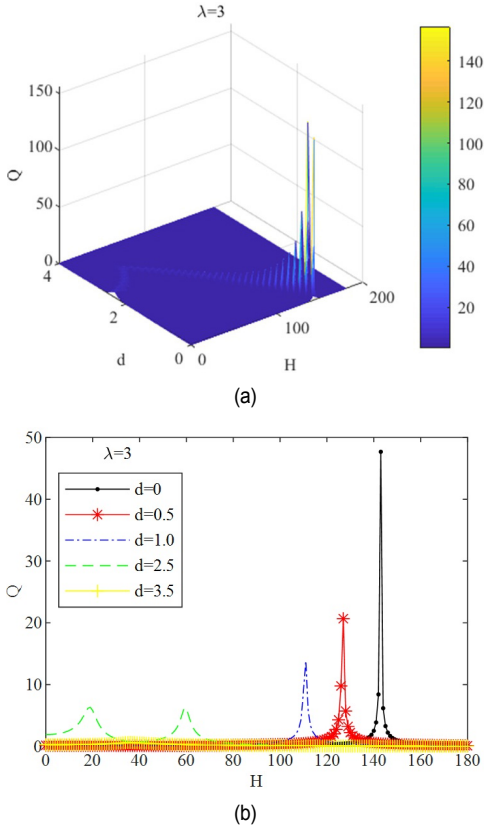

Fig. 2. Variation of the response amplitude Q with H and d when $A=0.1$, $f_0=0.01$, $f_h=1$, $\lambda=3$, and $a_0=b_0=1$: (a) analytical results of the response amplitude Q versus H and d; (b) response amplitude Q versus H for different values of d.

with an increase in γ. Fig. 1(c) shows that the resonance peak Q decreases with an increase in the value of $|d|$, indicating that when $|d|$ is smaller, the VR phenomenon is more obvious. In addition, the amplitude $|d|$ of driving high-frequency signals corresponding to each maximum Q value increases with an increase in the value $|d|$, indicating that when the auxiliary driving signal amplitude H is larger, VR can be induced by the acceleration of the composite influence factor $|d|$. For different attenuation coefficients of λ, selecting a reasonable compound influence factor $|d|$ can induce VR.

Similar to the classical Duffing study of VR, Fig. 2 shows the analysis results for the fixed λ. A smaller d indicates a more evident VR effect and larger amplitude H of the driving high-frequency signal. Fig. 2(a) shows that two VRs occur when d is slightly lower than λ, and the possibility of resonance at that time decreases sharply when $d>\lambda$ is used ($\lambda>\gamma$). In Fig. 2(b), when d = 3.5 is used, the peak value of Q decreases sharply, which is significantly lower than the peak value of Q with d = 2.5.

Figs. 1 and 2 show that the attenuation coefficient λ and damped ratio γ can cooperate to induce the occurrence of an attenuation oscillation signal VR. For small-parameter λ, we can always find an appropriate γ to induce the VR phenomenon.

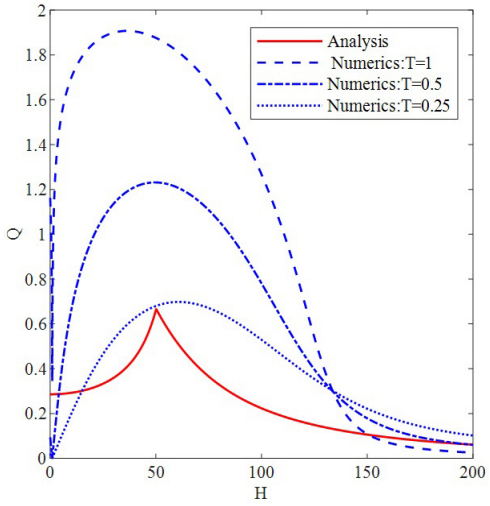

Fig. 3. Dependence of Q on H for analysis and different values of T (= 1, 0.5, 0.25). Analytical (solid lines) calculated from Eq. (7) and numerical (broken lines) from Eq. (8). Parameters are as follows: $A=0.1$, $f_0=0.01$, $f_h=1$, $\lambda=3$, $\gamma=2.5$, $a_0=1$ and $b_0=0.5$.

In the numerical analysis, to quantify the amplification of weak damped oscillation signals through a nonlinear system, an index called response amplitude Q at frequency f_0 input signal is defined [18] as follows:

$$Q=S/\mathrm{A} \tag{8}$$

where $S=\sqrt{B_s^2+B_c^2}$, $B_s=\frac{2}{nT}\int_0^{nT}x(t)\sin(\omega t)dt$, $B_c=\frac{2}{nT}\int_0^{nT}x(t)\cos(\omega t)dt$, and $T=\frac{2\pi}{\omega}$, n (= 1, 2, 3 …) is any positive integer. The fourth-order Runge-Kutta (FORK) scheme was used to solve the numerical solution of system (1) with a discrete signal of $s(t)$ and $H\cos(2\pi f_h t)$.

For a small value of λ, according to the previous analysis results, the corresponding γ induced VR can always be found. The analysis value is far from the numerical analysis and has no practical application value in $d\le\lambda$. Here, we consider $\lambda>\gamma$. Fig. 3 shows the theoretical Q calculated using Eq. (12) and the value Q obtained from Eq. (13). These display superposition response curves depict the dependence of the response amplitude Q of the theoretical analysis value and three other numerical values of different impact periods T (= 1, 0.5, 0.25) on the amplitude H of the high-frequency signal. The continuous line represents the response curve of the theoretical analysis Q value, whereas the dotted lines represent the corresponding numerical values. The other parameter values are fixed as A = 0.1, f_0 = 0.01, f_h = 1, λ = 3, γ = 2.5, a_0 = 1 and b_0 = 0.5. By changing the amplitude of the fast signal, system (1) was driven into the resonance state. The analytical values and numerical analysis show that they exhibit

the same trend. Here, we can observe that in contrast to the analysis value of Eq. (12), the height of the peak value is determined by the size of the impact period in the numerical analysis. VR does not occur when the impact period of T is very small (i.e., the impact frequency is relatively large). Therefore, the theoretical calculation results are consistent with the results of some numerical calculations. With a reduction in the impact period, the peak value also decreases, indicating that the impact frequency of the damped oscillation signal must also satisfy the small-parameter condition (usually on the order of 1).

2.2 Method of VMD

However, VR has a certain noise reduction ability [12] because of the strong noise frequency interference in the working environment of the combine harvester, and reducing the noise of the output signal of the VR system is sometimes necessary.

EMD is a good decomposition method for dealing with nonlinear and nonstationary signals, but mode aliasing is a serious problem. However, VMD is an adaptive signal-processing method proposed by Dragomiretskiy et al. [20] in 2014. The iterative search for the optimal solution of the variational mode is a completely nonrecursive signal decomposition method based on the frequency domain, which overcomes many shortcomings of EMD to a certain extent. It decomposes an actual complex signal into several modal functions with specific sparse characteristics. The instantaneous frequency of decomposing each analytical signal has a practical physical significance. The decomposition accuracy and noise resistance are better than those of EMD; however, the number of decompositions must also be defined. All decomposed modes include the modes of the main signals and noise. The modes of the main signals are reconstructed to achieve denoising. VMD has been applied to bearing fault diagnosis [21], noise reduction, and the extraction of weak signals [22].

3. VR numerical method for high-frequency weak characteristic damped oscillation signal

Similar to the SR theory, classical VR theory must satisfy the small-parameter condition. The system parameters are very small (generally less than the order of magnitude of one), and the frequency of the characteristic signal is low (generally much less than the order of magnitude of one). The oscillation frequency of the high-frequency weak characteristic signal can hardly satisfy the requirements of low frequency; therefore, scale transformation must be carried out initially to reduce the signal frequency. Because the weak characteristic signal may be distorted after downsampling of the high-frequency signal, this study adopts the parameter normalization transformation method provided in the Ref. [23]. For $f_0 >> 1$, we scale the following high-frequency system (9):

$$\frac{d^2x(t)}{dt^2}=ax(t)-bx^3(t)-\gamma\frac{dx(t)}{dt}+ Ae^{-\lambda(t-nT)}\sin(2\pi f_0 t)+H\cos(2\pi f_h t) \tag{9}$$

The two substitution variables $x(t)=z(\tau)$ and $\tau=mt$ are introduced, where m is the proportion parameter, and τ is a new time scale. After substituting them into Eq. (9), we obtain the following scale-transformation Eq. (10):

$$\frac{d^2z(\tau)}{d\tau^2}=\frac{a}{m^2}z(\tau)-\frac{b}{m^2}z^3(\tau)-\frac{\gamma}{m}\frac{dz(\tau)}{d\tau} +\frac{A}{m^2}e^{-\lambda(\tau-nT)/m}\sin(\frac{2\pi f_0}{m}\tau)+\frac{H}{m^2}\cos(\frac{2\pi f_h}{m}\tau) \tag{10}$$

Let $a_1=\frac{a}{m^2}$, $b_1=\frac{b}{m^2}$, $\gamma_1=\frac{\gamma}{m^2}$, $\lambda_1=\frac{\lambda}{m}$, $T_1=\frac{T}{m}$, $A_1=\frac{\lambda}{m^2}$, $H_1=\frac{H}{m^2}$, $\omega_1=\frac{2\pi f_0}{m}$ and $\varphi_1=\frac{2\pi f_h}{m}$. Then, Eq. (10) is converted to Eq. (11):

$$\frac{d^2z(\tau)}{d\tau^2}=a_1z(\tau)-b_1z^3(\tau)-\gamma_1\frac{dz(\tau)}{d\tau} +A_1e^{-\lambda_1(\tau-nT_1)}\sin(\omega_1\tau)+\frac{H}{m^2}\cos(\varphi_1\tau) \tag{11}$$

Comparing Eq. (11) with low-frequency system (1), when m is sufficiently large, the high-frequency $f_0 >> 1$ and impact frequency $\frac{1}{T}$ are reduced to $\frac{1}{m}$ of the original one, which can satisfy the low-frequency requirement of VR. Therefore, the excitation signal in Eq. (11) has the same time scale as that of the low-frequency system (1). A suitable m is selected such that the system parameter in Eq. (11) and the system parameter in the low-frequency system (1) have the same value or the same level of value (usually the order of magnitude of 1). Therefore, when system (9) reaches the matching condition of VR, the signal and system parameters in Eq. (11) are selected according to Eq. (1) of the system. At the same time, compared with system (9) of the high-frequency system, the amplitude of the auxiliary drive signal is reduced to the $\frac{1}{m^2}$ of the original signal, and the frequency is reduced to the $\frac{1}{m}$ of the original signal. The signal amplitude must be restored to the original intensity to enable Eq. (11) to have the same dynamic characteristics as the high-frequency system (9). Therefore, Eq. (12) is equivalent to system (9) in the time scale τ, as follows:

$$\frac{d^2z(\tau)}{d\tau^2}=a_1z(\tau)-b_1z^3(\tau)-\gamma\frac{dz(\tau)}{d\tau} +Ae^{-\lambda_1(\tau-nT_1)}\sin(\omega_1\tau)+H\cos(\phi_1\tau) \tag{12}$$

Simultaneously, in the project, frequency reduction process-

ing after the actual sampling of high-frequency signals may lead to data distortion. In the time scale t, system (13) is established after restoring the small frequency in Eq. (12) to large parameters. Therefore, when system (13) resonates, VR can occur in the high-frequency damped oscillation signal.

$$\frac{d^2x(t)}{dt^2}=ax(t)-bx^3(t)-m\gamma\frac{dx(t)}{dt}+ m^2Ae^{-\lambda(t-nT)}\sin(2\pi f_0t)+m^2H\cos(2\pi f_ht) \tag{13}$$

The damped oscillation simulation signal $s(t)=Ae^{-\lambda(t-nT)}\sin(2\pi f_0t)$ is given, in which A = 0.2, λ = 30, f_0 = 100 Hz, T = 2, n = 24, γ = 0.0223 separately. The frequency f_h of the high-frequency drive excitation signal $H\cos(2\pi f_ht)$ shall satisfy the condition of $f_h >> f_0$. f_h = 1700 Hz and other frequencies are also appropriate, as long as the above condition is satisfied. System parameters take a_1 = 0.0478 and b_1 = 6.0718e-04. Finally, the appropriate parameter value m is selected, but is not unique, as long as it can reduce the characteristic frequency, which is m = 5652 here. Fig. 4(a) shows the amplitude H = 0.9 of the driving signal and the optimal response amplitude Q = 5.0254 when VR occurs. Fig. 4(b) shows the original time domain waveform of the simulation signal, and Fig. 4(c) shows the time domain waveform of the system output when VR occurs. Some initial points are deleted to obtain the stable response for calculation to eliminate the influence of transient response. Comparing Figs. 4(b) and (c), the response peak of weak damped oscillation signal has been significantly amplified, showing that VR has excellent effect on processing and amplifying the simulated damped oscillation signal.

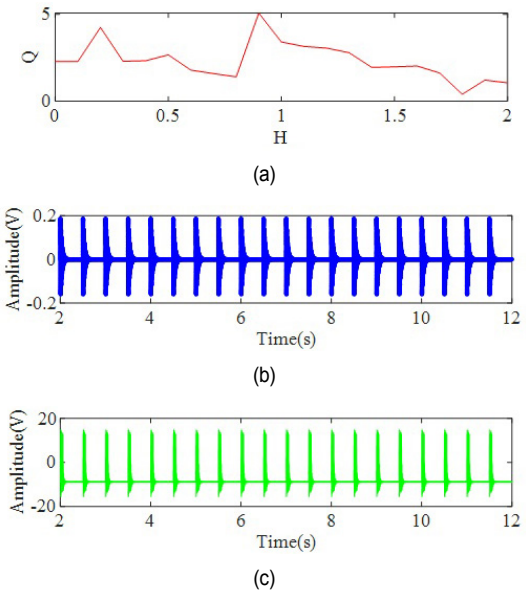

Fig. 4. VR output effect of high-frequency noiseless simulation signal of damped oscillation for $A=0.2$, $\lambda=30$, $f_0=100$ Hz, $T=2$, $n=24$: (a) Q versus H; (b) original simulation signal; (c) VR system output signal.

4. Adaptive extraction method of oscillation damped signal based on VR-VMD under noise background

In Secs. 1 and 2, the VR theory of the damped oscillation signal was studied in a second-order Duffing system, and the simulation analysis verified that the VR theory can amplify the amplitude of the damped oscillation signal. However, the Q index of VR response amplitude is generally applicable to weak noise or clean signals. When the noise environment is relatively poor, other detection indices should be constructed according to the characteristics of the damped oscillation signal. Based on the VR theory of weak characteristic damped oscillation signals, in this section, the adaptive extraction method in an agricultural machinery operation environment is studied.

4.1 Detected evaluation index

The kurtosis index K is highly sensitive to the impact component of a signal. As a dimensionless index, the kurtosis index is unaffected by the absolute level of the signal and is highly sensitive to the impact component of the signal. This method is suitable for the detection of a single impact signal. This is defined as the ratio of the fourth-order moment of the signal to the square of the second-order moment. The damped oscillation signal can be considered a combination of multiple amplitude-damped single-impact signals, and the detection result of a single damped oscillation signal tends to be an independent steep pulse. The cross-correlation coefficient C quantitatively represents the similarity between the input and output signals. Therefore, the weighted kurtosis index $Kc=K*|C|$ of the comprehensive cross-correlation coefficient can be used to detect noisy damped oscillation signals [24, 25].

4.2 VR effect of antinoise

To measure the noise reduction effect of VR, the SNR index is used to measure the output curve of VR and SR with the change of noise intensity. The antinoise performance analysis results are shown in Fig. 5. The damped oscillation simulation signal parameters were set. The noise signal was added to the weak damped oscillation simulation signal, and the statistical characteristics of the noise satisfy the conditions of $N(t)=\sqrt{2D}\zeta(t)$ and the noise intensity D, which $\zeta(t)$ is Gaussian white noise with $\langle\zeta(t)\zeta(t')\rangle=2D\delta(t-t')$ and mean $\langle\zeta(t)\rangle$ = 0. D from 0.05 to 20 with a step size of 0.05. Fig. 5 shows that the SNR decreased with an increase in D. When H = 0 there is no high-frequency drive signal (i.e., SR system), its SNR value is significantly lower than another H value (i.e., VR system). The experiment shows that the noise reduction effect of VR output is better than that of SR output. Although Fig. 5 also shows the attenuation trend, the VR output has a certain effect on the SNR of the damped oscillation signal. This

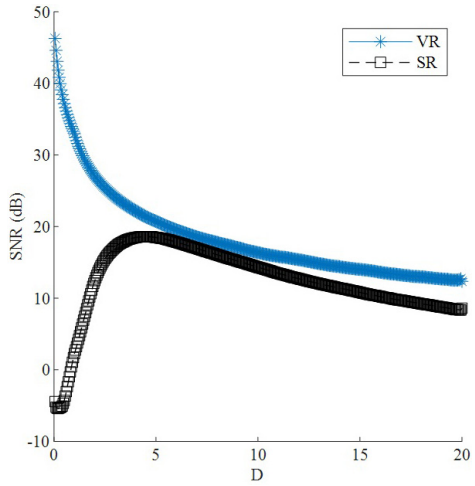

Fig. 5. Performance analysis curve of noise suppression using the VR method when $A=0.2$, $\lambda=30$, $f_0=100$ Hz, $T=2$, $n=24$.

demonstrates some antinoise ability.

4.3 VR-VMD adaptive extraction method based on quantum particle swarm optimization (QPSO)

QPSO is an optimization algorithm that combines quantum computing with particle swarm optimization. This greatly improves the search efficiency [26]. This algorithm is simple and easy to implement in practical applications. Parameter optimization of the VR adaptive system based on the weighted kurtosis index Kc is expressed as follows:

$$\begin{aligned} &\textbf{Maximize} \quad Kc(a_1,b_1,\gamma,H) \\ &\textbf{Subject to} \quad a_1\in(0,1)\,,\, b_1\in(0,1) \\ &\qquad\qquad \gamma\in(0,2)\,,\, H\in(0,1) \end{aligned} \tag{14}$$

The parameters of the attenuation oscillation signal are set to A = 0.2, λ = 50, f_0 = 100 Hz, T = 2, and n = 24, and the time domain waveform is shown in Fig. 6(a). To obtain more practical applications, the simulated signal lacks two cycles of damped oscillation signals. The noise signal is added to the weak damped oscillation simulation signal, and Gaussian white noise is considered in D = 0.01. A noisy simulation signal is shown in Fig. 6(b). Set f_h = 1700 Hz and m = 5652. As shown in Fig. 6(c), the optimal values of the QPSO parameters after 100 iterations were a_1 = 0.2265, b_1 = 0.2027, γ = 1.3310, and H = 0.1002. These optimal parameters were substituted into the large parameter bistable second-order VR Eq. (18), and the results are shown in Fig. 6(c). The impact pulse in the noise can be identified to a certain extent from Fig. 6(c). Fig. 5 shows that the noise reduction effect of VR on the noisy damped oscillation signal evidently weakens with an increase in noise intensity D. Therefore, secondary noise reduction processing is required in the background of strong noise. The effect of VMD decomposition is mainly affected by the selected

Table 1. Center frequency corresponding to different k.

k	Frequency / Hz				
3	38	100	609	-	-
4	38	100	494	1699	-
5	26	100	397	753	1699

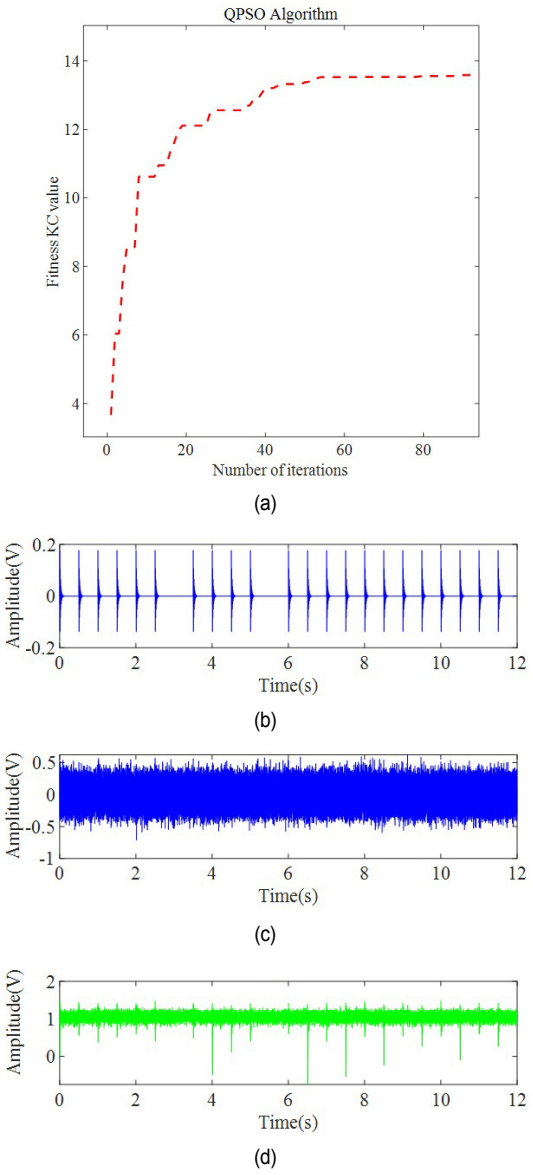

Fig. 6. Adaptive VR output effect of noisy simulation signal fixed parameters $A=0.2$, $\lambda=50$, $f_0=100$ Hz, $T=2$, $n=24$: (a) QPSO algorithm for parameter optimization; (b) original simulation signal; (c) noisy simulation signal; (d) optimal VR output signal.

value k of modal number. Since the noisy simulation signal contains at least useful signal, noisy signal and trend term, so $k\geq 3$. The main difference of different modes lies in the difference of the center frequency. According to Table 1, $k=3$, 4 and 5 are OK. In consideration of the contrast effect between VR-VMD method and VMD direct decomposition of weak sig-

nals, k = 5 is set here. The VMD method decomposes the signal shown in Fig. 6(c), and the results are shown in Fig. 7. From the time domain and frequency domain of the third intrinsic mode function (IMF) in Fig. 7, the damped oscillation signal with a first peak frequency of 100 Hz can be identified, and the noise reduction effect is evident. To compare the noise reduction output effect of VR-VMD on the noisy damped attenuation signal, the VMD decomposition of the noisy signal in Fig. 6(c) was performed directly. The results are shown in Fig. 8. The damped oscillation signal cannot be identified from the time and frequency domains of each modal component, as shown in Fig. 8. VMD has no direct noise-reduction ability for high-frequency damped oscillation signals in a strong random noise background. The comparison between Figs. 8 and 7 shows that VR has a certain energy enhancement effect on the high-frequency damped oscillation signal in a noisy environment, and VMD can realize a noise reduction function.

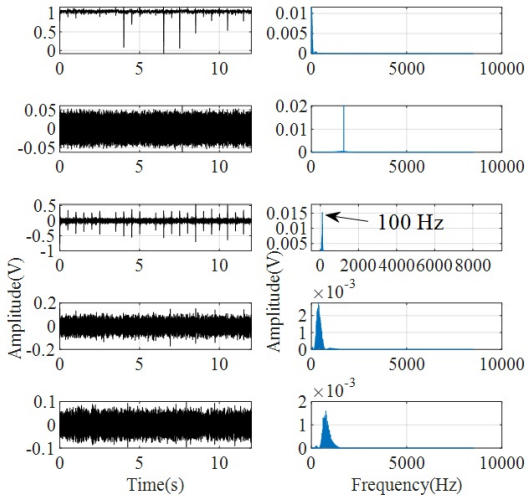

Fig. 7. VMD decomposition effect after VR output of Fig. 6(d).

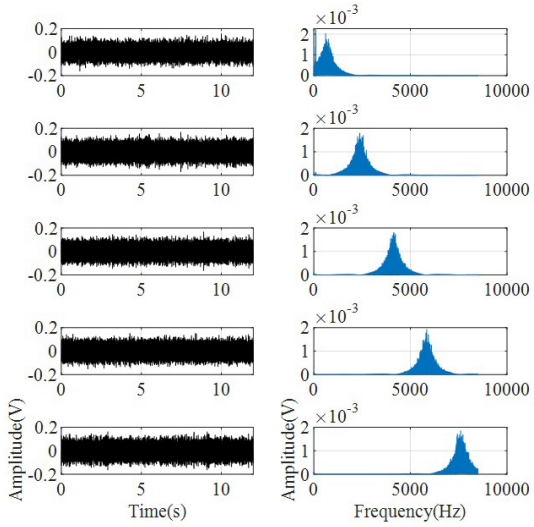

Fig. 8. Effect of direct VMD decomposition of original noisy simulation signal.

5. VR-VMD application and result analysis in the agricultural machinery working environment

In this section, an experiment in an agricultural machinery operation environment is used to evaluate and compare the performance of VR-VMD and HHT envelope analysis. The envelope detection method [27, 28] is a traditional method for detecting and discriminating grain losses.

5.1 Detection theory of piezoelectric loss sensor

When an external force is applied to the piezoelectric element to produce mechanical deformation, it causes a relative movement of its internal positive and negative charge centers to produce electrical polarization, resulting in bound charges with opposite polarities on the two surfaces of the element. The charge density is directly proportional to the external force. This phenomenon is known as the positive piezoelectric effect. A positive piezoelectric effect indicates that piezoelectric materials transform mechanical energy into electrical energy. Therefore, by detecting the charge transformation on the piezoelectric element, we can determine the deformation of the grain-impact vibrating plate, and the piezoelectric material can be made into a grain-loss pickup sensor by using the positive piezoelectric effect.

When different materials are used to impact a piezoelectric loss sensor, the signal frequencies are different [29]. They reflect high frequency and large amplitude for grains and stalks and low frequency and small amplitude for broken grass and stalks without stems. The interference signals, such as broken grasses and stems, through the band-pass filter circuit (Fig. 9 shows the tradi-

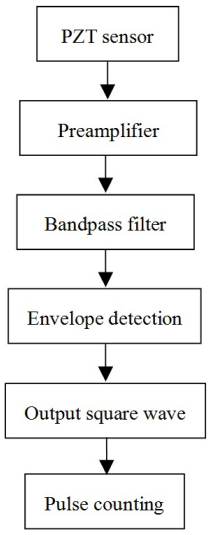

Fig. 9. Flow chart of traditional piezoelectric loss signal processing circuit.

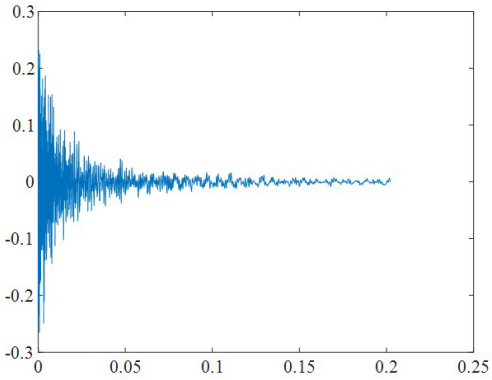

Fig. 10. Typical output voltage waveform by piezoelectric sensor impact of the rice grain.

tional signal-processing circuit) should be removed. It is often unable to detect the signal loss because this method does not consider the influence of strong noise in the agricultural machinery environment, especially in the time domain.

Fig. 10 shows a typical output voltage waveform of the piezoelectric sensor, which was generated by a single impact of the grain. Ignoring the particle size, the voltage amplitude increased with an increase in the impact height. The maximum value of the voltage signal also depended on the kinetic energy of the grain before impact. The waveform depended on the particle size. The output signal of the grain impact piezoelectric loss sensor is a typical damped oscillation signal, which can be expressed as follows [4]: $s(t) = Ae^{(-\lambda t)}\sin(2\pi f_0 t)$, where the signal amplitude is $A = \frac{F}{M\omega_d}e^{\xi\omega_n}$ (grain impact force F; grain mass M; ω_d is the natural frequency of the system damped vibration, which can be expressed as $\omega_d = \sqrt{1-\xi^2}\omega_n$, where ω_n is the natural frequency of the system undamped vibration); λ is the impact attenuation coefficient; and f_0 is the oscillation frequency of the grain-signal-impacting piezoelectric plate.

5.2 Experimental setup

To test the feasibility of this method in practical applications, an experiment on the impact of rice grain loss was carried out. Fig. 11 shows the structure and installation of the loss signal acquisition. The CI-yd-303 piezoelectric force sensor was fixed in the center of the aluminum plate, the response frequency was approximately 20 kHz, and the rectangular plate was 770 mm long and 600 mm wide. It is installed behind the cleaning sieve of the harvester. The collected experimental signal was transmitted to a notebook computer for storage through the YE7600 collector. We then read the data using MATLAB for signal processing and analysis.

5.3 Description of sensor signal processing process

The experimental data of the piezoelectric sensor were collected, and the VR-VMD algorithm was used to enhance and identify the weak impact signal of rice grains submerged in background noise. Fig. 12 shows the signal processing flow of the piezoelectric loss sensor based on the VR-VMD method. The specific method is described as follows.

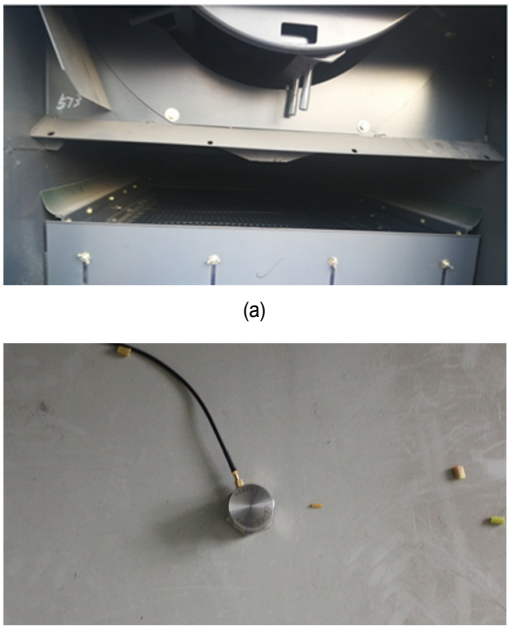

(a)

(b)

Fig. 11. Sensor installation on the combine: (a) cleaning sieve of harvester; (b) sensor installation structure.

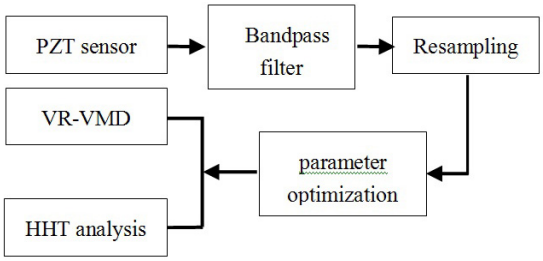

Fig. 12. Signal processing flowchart.

1) Signal preprocessing. The sensor always contains noise during the actual signal acquisition process. Thus, the collected sensor signal should be denoised to improve the SNR and signal quality, and then the denoised signal should be further analyzed. Irrelevant signals, such as chaff, broken stalks, and grasses, as well as the working vibration interference and machine noise of the harvester, affect the accuracy of loss signal detection. A band-pass filter was used to eliminate irrelevant interference and noise components as much as possible.

2) QPSO parameter initialization. The frequency of the auxiliary high-frequency signal is set to 17 times that of the oscillation signal, and the scale parameter m is set to nine times that of the oscillation angular frequency. Then, the search ranges of the adjustable parameters are initialized, as shown in Eq. (14).

3) Signal resampling. The preprocessed signal is resampled according to ten times the original sampling rate to be consistent with the sampling rate of the auxiliary high-frequency signal.

4) Determining the optimal parameters and maximum Kc. The objective function is given by Eq. (14). When the number of search iterations is completed, the optimal parameters are obtained, and the fifth step is performed. Otherwise, the process returns to step (4).

5) VR system output. After obtaining the maximum Kc and optimal system parameter values, the optimal output signal of the VR system is obtained according to the optimal value.

6) Signal post-processing. Secondary noise reduction for the output signal of the VR system should be performed because of the strong background noise of the combination. The VR output must be initially down-sampled. Extremely fast down-sampling results in signal distortion. Here, a distributed down-sampling method was used. Then, the VR output after down-sampling was input to the VMD decomposition algorithm to extract the weak characteristics of the rice grain damped oscillation signal. Finally, the effect was compared to that of the HHT envelope extraction method.

5.4 Discussion

Fig. 13 shows the collected grain impact signal, including the noise in the combined working environment. The original signal sampling frequency was 48 kHz, and the distance between the grain and sensor was 40 cm. As shown in Fig. 13, owing to the influence of background noise, the grain impact signal was not evident in the time domain waveform of the signal. Noise is characterized by low-frequency disturbances, short-time pulses,

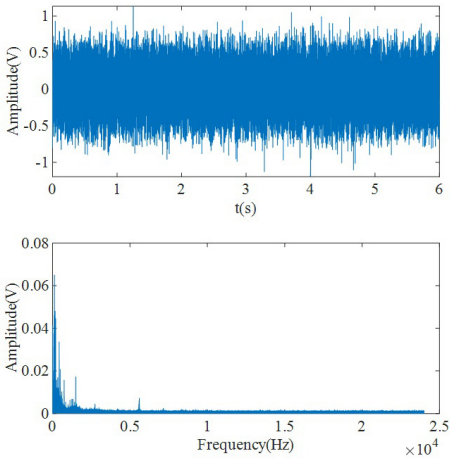

Fig. 13. Noise loss signal collected in agricultural machinery working environment.

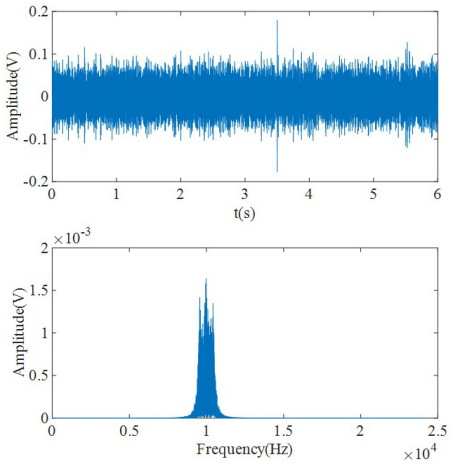

Fig. 14. Output effect of bandpass filter of noise loss signal collected in agricultural machinery working environment.

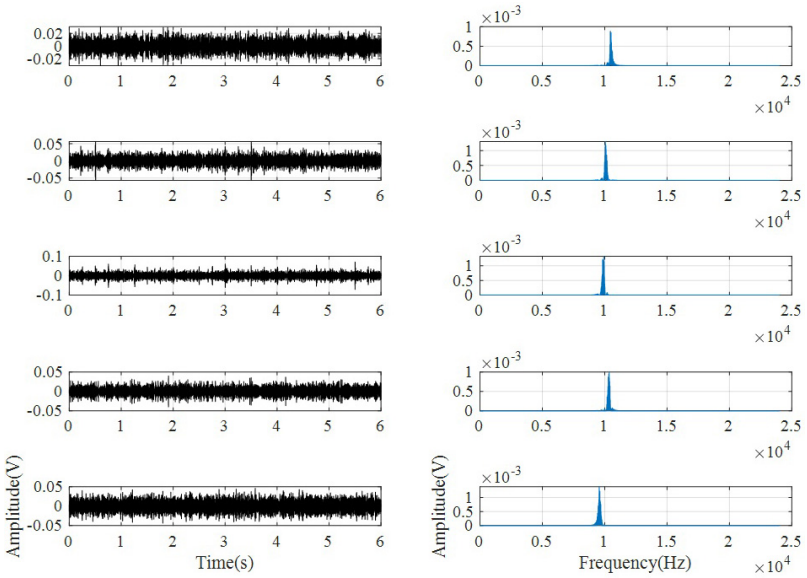

Fig. 15. VMD decomposition effect for Fig. 14.

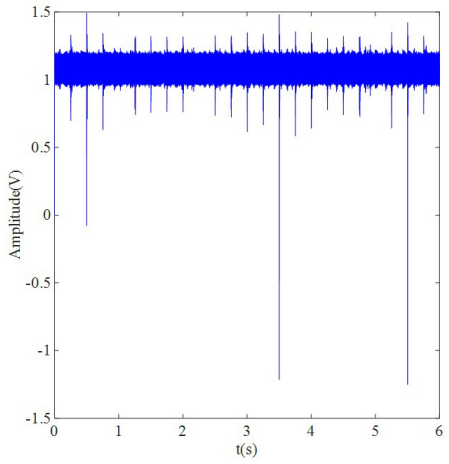

Fig. 16. VR output effect of in agricultural machinery working environment.

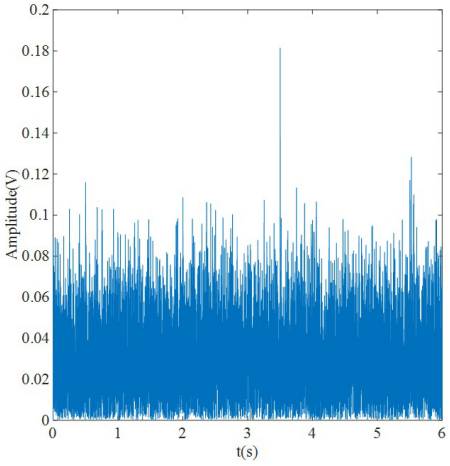

Fig. 18. HHT envelope extraction method.

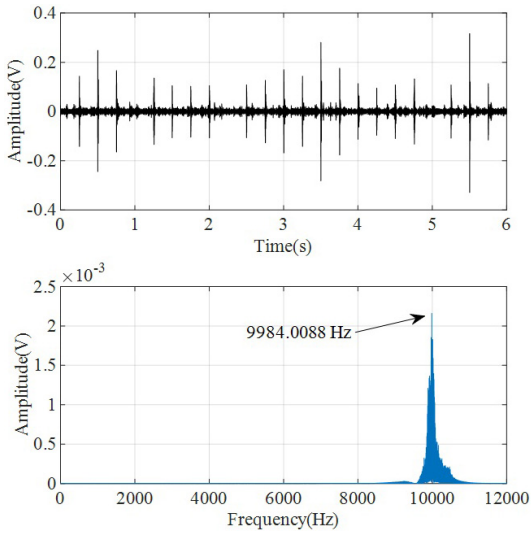

Fig. 17. The time domain and frequency domain of the fifth modal decomposed of the VR output signal in VMD algorithm in agricultural machinery working environment.

and high-frequency disturbances, with wide frequency coverage and certain diversity. The filtering results are shown in Fig. 14 after the original noisy signal passed through a bandpass filter with a center frequency of 10 kHz. The filtered signal was directly decomposed by VMD, and the results are shown in Fig. 15. From them, the impact amplitudes of rice impact are almost far less than 0.1 V and submerged in background noise.

The resonance frequency of the grain-damped oscillation was approximately 10 kHz in Fig. 14 and the auxiliary cosine signal frequency was added. Thus, the filtered signal in Fig. 14 must first be resampled to increase the sampling frequency of the filtered signal to ten times that of the original signal. The filtered signals were then processed using the proposed VR method. The variable scale coefficient m is set to 565200, and the optimization interval of other parameters a_1, b_1, γ and H are the same as the simulation signal. The output results of VR are shown in Fig. 16.

Before VMD noise reduction, it is necessary to reduce the frequency of the VR output to reduce the amount of computation of the VMD algorithm. First, the sampling frequency of the VR output signal was restored to 48 kHz. The second frequency reduction coefficient was set to 2. After two downsampling steps, the VR output results began the VMD decomposition. The detected rice grain loss signals are shown in Fig. 17. From the time and frequency domains of the fifth IMF in Fig. 17, the damped oscillation signal with the first peak frequency of 9984.0084 Hz can be identified. The figure shows that this signal contained 20 grain shocks. Subsequently, by setting the voltage threshold, the losses of the rice grains were easily detected in the time domain. As shown in Fig. 18, the conventional envelope method cannot identify the rice loss signal, but the proposed VR-VMD recognition and detection method has a certain recognition effect, which verifies its feasibility in practical applications.

6. Conclusions

A VR-VMD method based on a second-order Duffing bistable system was introduced to realize energy enhancement and noise reduction recognition of high-frequency weak characteristic damped oscillation signals under the background of strong noise in the agricultural machinery environment. The VR phenomenon of a weak damped oscillating signal in a second-order Duffing bistable system with low-frequency characteristics is theoretically presented using the direct motion separation method. The results show that coordination with the Duffing damping ratio and attenuation coefficient can induce VR for weakly damped oscillating signals. Then, from the practical application, the VR numerical analysis of the high-frequency weak feature damped oscillation signal is realized by the scale transformation method, which can effectively amplify the amplitude of high-frequency weak features. However, the response amplitude index is more suitable for the detection of high-frequency weak-feature signals without noise or weak noise. The noise reduction effect of the VR output decreases

with an increase in noise intensity owing to the strong noise background of the agricultural machinery operating environment. The VMD method was used to carry out secondary noise reduction for the VR system output, and a VR-VMD adaptive extraction method based on weighted kurtosis parameter optimization was proposed.

Through simulation and experimental analysis, this method can effectively suppress other useless frequency components in the background noise of agricultural machinery operation, so identifying the weak characteristic frequency of oscillation becomes easy. In addition, the VR-VMD method was compared with traditional envelope extraction analysis. The results show that the proposed method is effective and superior to envelope analysis against the background of agricultural machinery noise. The VR-VMD method provides some reference values for weak characteristic damped oscillation signal extraction, which is not limited to the agricultural machinery operating environment. Compared with the noise in SR, VR controls the auxiliary signal added to the environment of agricultural machinery operation noise more easily, and the large noise is difficult to eliminate in the environment of agricultural machinery operation. However, the parameters of the auxiliary signal can easily be changed.

Acknowledgments

This work was supported in part by the Science and Technology Innovation Project of the Chinese Academy of Agricultural Sciences (2015-2021) , Sichuan Province Key R&D Plan (2022YFG0079) and Jiangsu Agricultural Science, Technology Innovation & Promotion Fund Project (No.2020-16).

Nomenclature

VR	: Vibration resonance
VMD	: Variational mode decomposition
f_0	: Frequency of weak signal
λ	: Attenuation coefficient of weak signal
γ	: Damping ratio of the duffing oscillator
H and f_h	: Amplitude and frequency of high-frequency excitation periodic signal
a_0 and b_0	: Two parameters of the low-frequency system
a and b	: Two parameters of the high-frequency system
d	: Compound influence factor
QPSO	: Quantum particle swarm optimization
Kc	: Weighted kurtosis index
k	: Number of VMD decomposition

References

[1] R. Myhan and E. Jachimczyk, Grain separation in a straw walker unit of a combine harvester, *Process Model, Biosystems Engineering*, 145 (2016) 93-107.

[2] M. Omid, M. Lashgari, H. Mobli, R. Alimardani, S. Mohtasebi and R. Hesamifard, Design of fuzzy logic control system incorporating human expert knowledge for combine harvester, *Expert Systems with Applications*, 37 (10) (2010) 7080-7085.

[3] N. Jun, M. Hanping, Z. Xiaodong and C. Xiuhua, Application of butterworth filter for testing grain cleaning loss, *Transactions of the Chinese Society for Agricultural Machinery*, 41 (6) (2010) 172-176.

[4] G. Jianmin, Z. Gang, Y. Lu and L. Yangbo, Chaos detection of grain impact at combine cleaning loss sensor, *Transactions of the Chinese Society for Agricultural Engineering*, 27 (9) (2011) 22-27.

[5] M. Hanping, L. Wei, H. Lühua and Z. Xiaodong, Design of intelligent grain cleaning losses monitor based on symmetry sensors, *Transactions of the Chinese Society for Agricultural Engineering*, 28 (7) (2012) 34-39.

[6] M. R. Aslani, M. B. Shamsollahi and A. Nouri, Improving data protection in BSS based secure communication: mixing matrix design, *Wireless Networks*, 2 (7) (2021) 4747-4758.

[7] D. Paliwal, A. Choudhury and T. Govardhan, Detection of bearing defects from noisy vibration signals using a coupled method of wavelet analysis followed by FFT analysis, *Journal of Vibration Engineering and Technologies*, 5 (1) (2017) 21-34.

[8] M.-T. Shih, F. Doctor, S.-Z. Fan, K.-K. Jen and J.-S. Shieh, Instantaneous 3D EEG signal analysis based on empirical mode decomposition and the hilbert-huang transform applied to depth of anaesthesia, *Entropy*, 17 (3) (2015) 928-949.

[9] S. Wang, B. Lu, J. Cao, M. Shen, C. Zhou and Y. Feng, Research on a method for diagnosing clogging faults and longitudinal axial flow in the threshing cylinders of drum harvesters, *Noise Control Engineering Journal*, 69 (3) (2021) 209-219.

[10] R. Benzi, A. Sutera and A. Vulpiani, The mechanism of stochastic resonance, *Journal of Physics A: Mathematical and General*, 14 (1981) 453-457.

[11] P. S. Landa and P. V. E. McClintock, Vibrational resonance, *Journal of Physics A: Mathematical and General*, 33 (45) (2000) L433-L438.

[12] V. N. Chizhevsky and G. Giacomelli, Improvement of signal-to-noise ratio in a bistable optical system: comparison between vibrational and stochastic resonance, *Physical Review A*, 71 (1) (2005) 1-4.

[13] J. J. Thomsen, *Vibrations and Stability: Advanced Theory, Analysis, and Tools*, 2nd Ed. Springer, Berlin, German (2003).

[14] I. Blekhman, *Vibrational Mechanics: Nonlinear Nynamic Effects, General Approach, Applications*, World Scientific, Singapore (2000).

[15] J. H. Yang and H. Zhu, Bifurcation and resonance induced by fractional-order damping and time delay feedback in a Duffing system, *Communications In Nonlinear Science And Numerical Simulation*, 18 (5) (2013) 1316-1326.

[16] I. I. Blekhman and P. S. Landa, Conjugate resonances and bifurcations in nonlinear systems under biharmonical excitation, *International Journal of Non-Linear Mechanics*, 39 (3) (2004) 421-426.

[17] S. Ghosh and D. S. Ray, Nonlinear vibrational resonance, *Physical Review E*, 88 (4) (2013) 042904.

[18] J. P. Baltanas, L. Lopez, I. I. Blekhman, P. S. Landa, A. Zaikin,

J. Kurths and M. A. F. Sanjuan, Experimental evidence, numerics, and theory of vibrational resonance in bistable systems, *Physical Review E*, 67 (6) (2003) 066119.
[19] Y. Liu, Z. Dai, S. Lu, F. Liu, J. Zhao and J. Shen, Enhanced bearing fault detection using step-varying vibrational resonance based on duffing oscillator nonlinear system, *Shock and Vibration*, 2017 (2017) 1-14.
[20] K. Dragomiretskiy and D. Zosso, Variational mode decomposition, *IEEE Transactions on Signal Processing*, 62 (3) (2014) 531-544.
[21] X. Jiang, C. Shen, J. Shi and Z. Zhu, Initial center frequency-guided VMD for fault diagnosis of rotating machines, *Journal of Sound and Vibration*, 435 (2018) 36-55.
[22] W. Huang and D. Liu, Mine microseismic signal denosing based on variational mode decomposition and independent component analysis, *Journal of Vibration and Shock*, 38 (4) (2019) 56-63.
[23] D. Yang, Z. Hu and Y. Yang, The analysis of stochastic resonance of periodic signal with large parameters, *Acta Phys. Sin*., 61 (8) (2012) 50-59.
[24] Y. Cao, B. Yang, J. Yang, S. Zheng and W. Zhou, Impact signal adaptive extraction and recognition based on a scale transformation stochastic resonance system, *Journal of Vibration and Shock*, 35 (5) (2016) 65-69.
[25] X. Song, H. Wang and P. Chen, Weighted kurtosis-based VMD and improved frequency-weighted energy operator low-speed bearing-fault diagnosis, *Measurement Science and Technology*, 32 (3) (2021) 1-11.
[26] X. J. Gu and C. Z. Chen, Adaptive parameter-matching method of SR algorithm for fault diagnosis of wind turbine bearing, *Journal of Mechanical Science and Technology*, 33 (3) (2019) 1007-1018.
[27] Z. Zhao, Y. Li, J. Chen and J. Xu, Grain separation loss monitoring system in combine harvester, *Computers and Electronics in Agriculture*, 76 (2) (2011) 183-188.
[28] Z. Liang, Y. Li, L. Xu and Z. Zhao, Sensor for monitoring rice grain sieve losses in combine harvesters, *Biosystems Engineering*, 147 (2016) 51-66.
[29] G. Strubble, *Grain Loss Monitors for Harvesting Machines*, US5046362, Ford New Holland, USA (1991).

Suzhen Wang is a doctor of the Nanjing University of Science & Technology, China. She is also a researcher from Nanjing Research Institute for Agriculture Mechanization, Ministry of Agriculture and Rural Affairs, China. Her research interests include vibration signal analysis, driverless agricultural equipment and agricultural Internet of things technology.

Baochun Lu is a Professor at the Nanjing University of Science & Technology, China. His research interests include intelligent manufacturing and mechanical fault diagnosis.